Hindawi
Journal of Nanomaterials
Volume 2024, Article ID 9932000, 15 pages
https://doi.org/10.1155/2024/9932000

Research Article

Synthesis and Photocatalytic Activity of High-Quality Lead(II) Sulfide Nanoparticles from Lead(II) Thiosemicarbazone Complexes as Single Source Precursors

Adrien P. Yepseu,[1,2] **Thomas Girardet**,[2] **Linda D. Nyamen**,[1] **Solenne Fleutot**,[2] **Kevin I. Y. Ketchemen**,[1] **Walter N. Kun**,[1] **Franck Cleymand**,[2] **and Peter T. Ndifon**[1]

[1]*Department of Inorganic Chemistry, University of Yaoundé I, P.O. Box 812 Yaoundé, Cameroon*
[2]*Institut Jean Lamour UMR 7198 CNRS – Université de Lorraine, Nancy 54000, France*

Correspondence should be addressed to Franck Cleymand; franck.cleymand@univ-lorraine.fr and Peter T. Ndifon; pndifon@facsciences-uy1.cm

Received 18 August 2023; Revised 27 October 2023; Accepted 17 January 2024; Published 2 February 2024

Academic Editor: Fedlu Kedir Sabir

We report the synthesis of lead(II) complexes of 2-(thiophen-2-ylmethylene) hydrazine-1-carbothioamide (1) and 2-(1-(thiophen-2-yl) ethylene) hydrazine-1-carbothioamide (2), which were used as single source precursors in hexadecylamine (HDA) and oleylamine (OLA) at 190, 230, and 270°C to synthesize lead(II) sulfide nanoparticles. Optical studies by UV–vis analysis showed a general blue shift in the absorption band edge of the PbS nanoparticles (NPs) with energy bandgaps determined by Tauc's plots ranging from 2.15 to 3.11 eV. The development of NPs with a variety of morphologies that changed with temperature and precursor type was demonstrated by morphological characterization using scanning electron microscopy and transmission electron microscopy. Cubic, rod-shaped, and nearly spherical-shaped PbS were formed. Powder X-ray diffraction (p-XRD) structural studies revealed the face-centered cubic structure of PbS nanoparticles. The elements contained in the nanoparticles were identified by energy dispersive X-ray spectroscopy (EDX). These results suggest that the size, shape, and optical properties of the synthesized PbS NPs were affected by reaction temperature, capping group, and precursor type. Under UV irradiation, the photocatalytic activity of HDA-capped PbS nanoparticles on the degradation of methylene blue dye ranged from 28.3% to 60.0%, with lead sulfide nanoparticle obtained by thermolysis of complex (1) at 230°C showing the highest photocatalytic efficiency (60.0%).

1. Introduction

Recently, there has been a lot of interest in metal sulfide nanomaterials with various morphologies because of their special optical, chemical, and physical properties [1–5], as well as their potential uses as photocatalysts and in photovoltaic, optical, and optoelectronic devices [6–9]. PbS is a significant IV–VI semiconductor, having a relatively large exciton Bohr radius (18–20 nm) and a small bandgap (0.41 eV), which allows for good hole and electron quantum confinement in nanometer-sized structures [10]. The interest in lead sulfide nanoparticles is due to their interesting optical properties. These properties are strongly influenced by their morphology, phase, and surface characteristics, and the ability to control these properties by adjusting their size, shape, and phase will determine their potential use in a variety of applications, including gas detection, optical devices, photovoltaic cells, light-emitting diodes, and photocatalysis [5–17]. These interesting properties and applications of PbS nanomaterials have encouraged researchers to examine new synthetic methods and applications [11–17]. The morphologies of lead sulfide nanoparticles, including nanotubes, nanorods, nanosheets, and flower-like structures, can have a significant impact on their characteristics [18]. Many methods, including thermal decomposition of single source precursors (SSPs) and hydrothermal and solvothermal processes, used for the preparation of PbS nanoparticles of different morphologies, have been reported in the literature [12, 13–18]. One of the methods mentioned is the SSP route, which not only avoids environmental pollution and complex purification steps but also provides a straightforward, effective,

economical, and scalable approach to producing high-quality, monodispersed, crystalline semiconductor PbS nanomaterials [15–18]. The selection of metal complexes as single source precursors with preformed metal–chalcogenide bonds provides an appropriate reactive intermediate that enables the high-temperature synthesis of metal sulfide nanoparticles [18–20]. Thiosemicarbazone complexes have demonstrated their ability to yield high-quality metal sulfide nanomaterials among the different metal complexes that have been used as SSPs [21, 22]. The use of heterocyclic thiosemicarbazone complexes as SSPs for PbS nanoparticle preparation has received very little attention in the literature. In our previous study, we used copper(II) thiosemicarbazone complexes as SSPs for the preparation of Cu_9S_5 NPs and examined their application as effective photocatalysts for the degradation of methylene blue dye [21, 22]. In the present study, we thought it appropriate to study the effect of varying reaction parameters on the size, shape, and optical properties of PbS NPs using the same heterocyclic thiosemicarbazone ligands. As a result, high-quality PbS nanoparticles with varied shapes and good crystallinity were obtained. We therefore describe the synthesis of PbS NPs using two homoleptic lead(II) heterocyclic thiosemicarbazone complexes as SSPs. We have studied the size, shape, and optical characteristics of PbS NPs, in relation to the reaction temperature, solvent, and type of precursor. We also report our investigation on the photocatalytic degradation of methylene blue dye under UV irradiation using HDA-coated PbS nanoparticles.

2. Experimental Section

2.1. Chemicals. The following chemicals were purchased from Sigma–Aldrich Chemie (Hamburg, Germany), Merck (Darmstadt, Germany), and Codimed (Yaoundé, Cameroon) and used without further purification: oleylamine (OLA, 70%), hexadecylamine (HDA, 90%), lead acetate (99%), thiosemicarbazide (99%), 2-thiophenecarboxaldehyde (99%), 2-acethylthiophene (99%), methylene blue (99%), acetone (99%), methanol (99.5%), ethanol (99.5%), and toluene (99%).

2.2. Instrumentation. An automated Perkin-Elmer CHNS/O analyzer, model 2400 series II was used to perform elemental analyses (C, H, N, and S) of ligands and the corresponding lead(II) complexes. An analogy-SMP11 melting point measuring device of the Stuart Scientific type equipment was used to determine the melting points. To identify functional groups, ligand and complex IR spectra were recorded in the 4,000–450 cm^{-1}wave number range using a Perkin-Elmer Spectrum One FTIR spectrometer. For the thermal studies, thermogravimetric analysis was performed using a Perkin Elmer Pyris 6 Thermogravimetric Analysis device up to 600°C in a nitrogen atmosphere. An X'Pert MPD diffractometer was used to perform X-ray diffraction (XRD) measurements, and the radiation source used was Cu Kα radiation (λ = 1.5406 Å). A CM200-FEI was used to record images for transmission electron microscopy (TEM) at 200 KV, and a Quanta 650 FEG–FEI was used to record scanning electron micrographs. Using dither dispersive X-ray spectrometers (EDX system coupled with SDS), the elemental composition of the nanoparticles was determined at room temperature, an Ocean Optics FX-VIS-IRS-ES spectrophotometer was used to record the absorption spectra of the precursors and nanoparticles as well as the photodegradation of the methylene blue.

2.3. Preparation of the Ligands and Lead(II) Complexes. The method previously reported was used to synthesize and characterize the ligands, 2-thiophenecarboxaldehyde and 2-acetylthiophene thiosemicarbazone [22, 23]. A hot solution of ethanol (20 mL) containing $Pb(CH_3COO^-)_2$ (1.14 g, 3 mmol) was added dropwise to another hot solution of ethanol (20 mL) containing the corresponding ligand (1.10 g, 6 mmol) and the mixture heated to 80°C under reflux for 2 hr while stirring [22, 24]. The resultant precipitate was allowed to cool to room temperature before being filtered, cleaned in ethanol, and allowed to dry at room temperature.

$[Pb(C_6H_6N_3S_2)_2]$ (1). Yield: 55%, melting pt > 300°C. Analysis calculated for $[Pb\ (C_6H_6N_3S_2)_2]$: C, 25.03; H, 2.10; N 14.60. Found: C, 24.69; H, 1.80; N, 14.25. Important infrared bands (cm^{-1}): $\nu_{(NH2)}$: 3,455, $\nu_{(C=N)}$: 1,562, $\nu_{(N-N)}$: 1,076, $\nu_{(C-S)}$: 882, $\nu_{(M-N)}$: 494.

$[Pb(C_7H_8N_3S_2)_2].H_2O$ (2). Yield: 54%, m.pt. > 300°C. Analysis calculated for $[Pb\ (C_7H_8N_3S_2)_2].H_2O$: C, 27.04; H, 2.92; N 13.52. Found: C, 27.28; H, 2.62; N, 13.32. Important infrared bands (cm^{-1}): $\nu_{(NH2)}$: 3,423, $\nu_{(C=N)}$: 1,569, $\nu_{(N-N)}$: 1,034, $\nu_{(C-S)}$: 859, $\nu_{(M-N)}$: 514.

2.4. Synthesis of PbS Nanoparticles. A previously reported procedure was slightly modified to prepare lead sulfide nanoparticles [3, 22]. Three grams of the capping agent (OLA or HDA) were added to a three-neck flask fitted with a reflux condenser, thermometer, and rubber septum. The flask was then heated to the appropriate temperature (190, 230, or 270°C). Using a glass syringe, a suspension of complex (1) or complex (2) (0.20 g) dispersed in oleylamine (3.00 g) was injected into the heated oleylamine. After 30 min of stirring, the reaction mixture was allowed to cool to room temperature. A black precipitate of PbS NPs was obtained by adding ethanol to the mixture, and this precipitate was separated by centrifugation at 2,500 rpm for 10 min. Ethanol was used to wash the black residue three times. To examine the effect of the capping agent on the morphological and optical properties of the as-prepared PbS NPs, the same procedure was carried out using hexadecylamine (HDA). For spectroscopic analysis and isolation, the samples were dispersed in toluene.

2.5. Photocatalytic Activity. With minor modifications, a previously reported procedure [22, 25] was used to carry out the photocatalytic degradation of methylene blue dye using the as-synthesized HDA-capped PbS nanoparticles as photocatalysts. A 5 mg (10 ppm) methylene blue solution was prepared in a volumetric flask (500 mL) using distilled water. The catalyst (5 mg) was dispersed in 50 mL of methylene blue dye solution in a Pyrex beaker. The solution was stirred magnetically in the dark for 15 min before irradiation, to achieve adsorption–desorption equilibrium. The resulting solution was then exposed to ultraviolet (UV) light irradiation (λ > 300 nm) for 60 min. Aliquots were collected at a

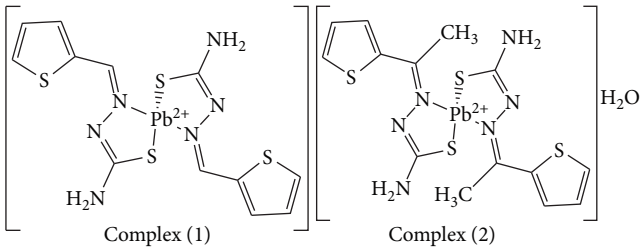

Figure 1: Suggested chemical structures of complexes.

15 min interval and a UV–vis–NIR spectrophotometer was used to read the UV–vis absorption of the clarified solutions after the photocatalyst had been separated from the mixed solution by centrifugation. The wavelength at which the maximum absorption of the MB solution was measured is 664 nm [25].

3. Results and Discussion

3.1. Characterization of Precursors. The synthesized ligands (L_1H, L_2H) and metal complexes ($[Pb(C_6H_6N_3S_2)_2]$ (1) and $[Pb(C_7H_8N_3S_2)_2]\cdot H_2O$ (2)) were obtained in good yields with the anticipated formulas. They are all colored and stable in air, and their nonelectrolytic nature is indicated by their respective molar conductance values of 11.1 and 23.0 $\Omega^{-1}cm^2\,mol^{-1}$ for complex (1) and complex (2) [17]. The proposed chemical structures of complexes are shown in Figure 1. Analytical data and physical properties of ligands and complexes are included in Table 1.

3.1.1. Infrared Study. Figure 2 shows the FTIR spectra of the ligands and the corresponding Pb(II) complexes. The FTIR spectra of the ligands L_1H and L_2H revealed bands at 1,582 and 1,594 cm^{-1} that corresponded to the azomethine group (C═N). This confirmed that the aldehyde or ketone fragment and the NH_2 group of thiosemicarbazide underwent a condensation reaction that produced the desired 2-(thiophen-2-ylmethylene) hydrazine-1-carbothioamide and 2-(1-(thiophen-2 yl) ethylidene) hydrazine-1-carbothioamide ligands [22, 26]. An analysis of the infrared spectrum of the ligand and those of the corresponding Pb(II) complexes shows a shift in the vibrational frequency of the —C═N— groups around 1,562 and 1,556 cm^{-1}, indicating that the metal ion and the nitrogen of the azomethine group (—C═N—) are coordinated. New bands at 494 and 514 cm^{-1}, which correlate to the nitrogen–metal (N–M) bond in lead complexes, also support this [22, 27]. The FTIR spectra of complex (1) and complex (2) do not contain the N—H bond vibration frequencies that are present in the FTIR spectra of ligands at 3,133 and 3,161 cm^{-1} [17]. The vibrations observed on the FTIR spectra of the complexes around 837 and 882 cm^{-1} show the presence of a band corresponding to the v(C—S) vibration, which suggests the formation of a metal–sulfur bond [17]. Furthermore, the water of crystallization is responsible for the band that appears in the complex (2) spectrum at about 3,304 cm^{-1}. Table 2 shows the significant vibrations in the FTIR spectra of ligands and complexes.

3.1.2. Electronic Spectra. The electronic spectra of the ligands and the corresponding Pb(II) complexes are shown in Figure 3. Three bands around 26,178 and 27,624 $cm-^{1}$ are visible in the ligands electronic spectra (Figure 3(a)). These bands result from the transitions $\pi \longrightarrow \pi^*$ (thiophene) and $n \longrightarrow \pi^*$ (thiosemicarbazone), respectively [25]. The shoulder around 24,390 cm^{-1} in the visible could be due to the possibility of thione–thiol tautomerism in the ligands. The electronic spectra (Figure 3(b)) of the complexes showed a band around 25,773 and 26,385 cm^{-1}, respectively. These absorption bands, which indicate the distinct colors (pale green and yellow light) and the tetrahedral geometry of the complexes, can be attributed to ligand–metal charge transfer (LMCT) [26]. The electronic spectra of the complexes show the presence of a band, which confirms that the ligand binds (S⟶M) to the Pb^{2+} ion via the sulfur atom.

3.1.3. Thermal Analysis of Precursors. The thermal stability of the complexes was confirmed by thermogravimetric analysis. Figure 4 shows the TGA curves for complexes (1) and (2) between 0 and 600°C in a nitrogen atmosphere. The thermal decomposition curve for complex (1) shows two decomposition steps. A loss of one ligand molecule (L1) is observed during the first decomposition step between 190 and 390°C, resulting in a weight loss of 31.9% (cal: 32.1%). The second weight loss of 16.4% (cal: 14.1%) occurs in the temperature range of 390–540°C and is caused by decomposition of the organic fraction of the second ligand molecule.

However, three decomposition stages are visible in the temperature range from 90 to 540°C on the TGA curve for complex (2). The first stage occurs between 90 and 120°C and corresponds to the loss of one molecule of water, i.e., 2.9% (cal: 2.9%). The second stage, with a weight loss of 32.1% (cal: 31.4%), takes place in the temperature range 210–380°C and corresponds to the degradation of one ligand molecule (L2). With a mass loss of 16.5% (cal: 15.8%), the third step, which takes place in the temperature range from 390 to 540°C, corresponds to the decomposition of the organic species of the second ligand molecule in the metal complex. Complex (1) and complex (2) yield 51.7% (calc: 53.8%) and 49.9% (calc: 48.5%) of PbS and carbon residues, respectively, as the final residues [28].

3.2. Structural and Morphological Studies of OLA-Capped PbS NPs

3.2.1. Structural Characterization for OLA-Capped PbS NPs. XRD was used to examine the phase composition and structure of OLA-capped PbS NPs using lead complexes (1) and (2) as precursors, as shown in Figure 5. According to JCPDS file number 01-071-4752, the results confirm the formation of the cubic phase of PbS (galena) with diffraction peaks at 2θ values of 27.37°, 30.09°, 34.90°, 50.30°, 59.81°, 62.78°, and 73.94° corresponding to the diffraction planes (111), (200), (220), (311), (222), (400), and (420). The sharpness of all the peaks suggests that the PbS NPs are crystalline. No extra peak was observed in the diffractograms of the PbS NPs suggesting that pure PbS materials were obtained by the

Table 1: Analytical data and physical properties for ligands (L_1H, L_2H) and its complexes.

Compound	Color	Melting point (°C)	Yield (%)	Molar conductivity (Ω^{-1} cm^2 mol^{-1})	Elemental analyses expt. (calc.)		
					C	H	N
$L_1H = C_6H_7N_3S_2$	Yellow	(182 ± 2)	69	—	38.69 (38.90)	4.33 (3.81)	22.56 (22.68)
$L_2H = C_7H_9N_3S_2$	Light yellow	(146 ± 2)	95	—	41.97 (40.82)	5.03 (4.79)	20.58 (20.17)
[Pb $(C_6H_6N_3S_2)_2$] (PbL_1(1))	Pale green	≥300	55	11.1	25.03 (24.69)	2.10 (1.80)	14.60 (14.25)
$[Pb(C_7H_8N_3S_2)_2]\cdot H_2O$ (PbL_2 (2))	Light yellow	≥300	54	23.0	27.04 (27.28)	2.92 (2.68)	13.52 (13.32)

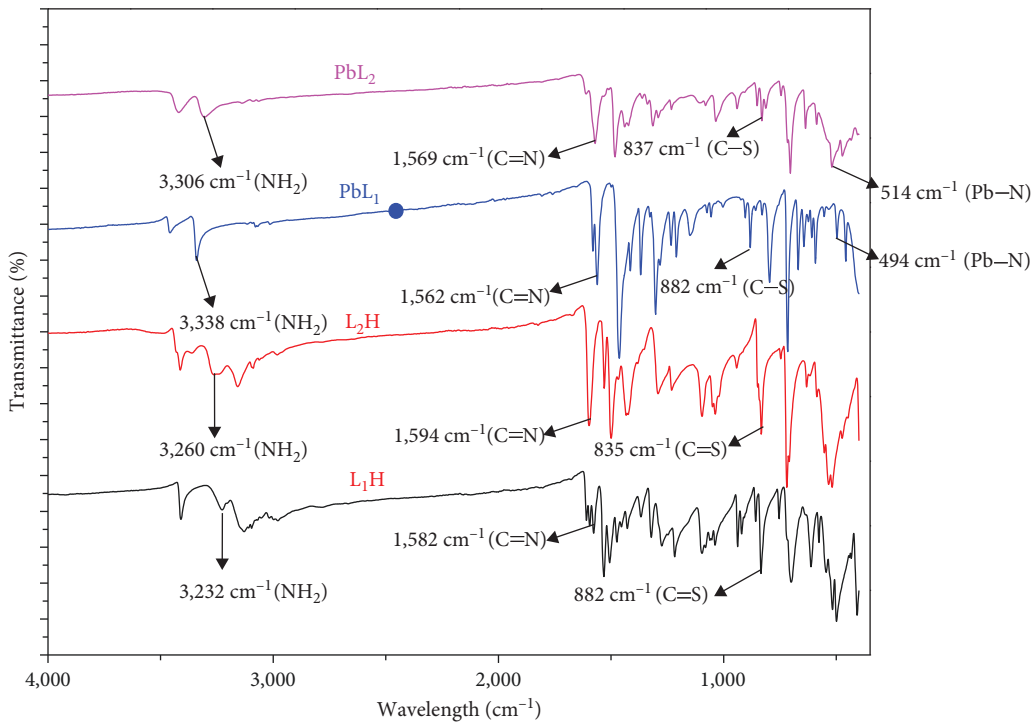

Figure 2: IR spectra of the L_1H and L_2H ligands and their corresponding PbL_1 and PbL_2 complexes.

Table 2: Infrared absorption bands for the ligands and the lead(II) complexes (cm^{-1}).

Compound	νNH_2	$\nu_{C=N}$	$\nu_{C=S}$	ν_{OH} (H_2O)	ν_{N-N}	ν_{C-S}	ν_{N-H}	ν_{Pb-N}
L_1H	3,410–3,232	1,582	835	—	1,044	—	3,133	—
L_2H	3,410–3,260	1,594	830	—	1,040	—	3,161	—
PbL_1 (1)	3,455–3,338	1,562	—	—	1,076	882	—	494
PbL_2 (2)	3,423–3,306	1,594	—	3,304	1,034	837	—	514

thermolysis of lead(II) thiosemicarbazone complexes. The results also show that increasing the thermolysis temperature (from 190 to 270°C) increases the crystallinity of the PbS nanoparticles, indicating that the reaction temperature has a direct impact on the crystallinity of the PbS nanoparticles. A similar result was reported for PbS NPs using the lead(II) ethyl xanthogenate complex [29]. Furthermore, it was found that changing the type of precursor had no effect on the crystalline phase of PbS nanoparticles. The Debye–Scherrer equation [30] was used to calculate the average crystallite size at 190, 230, and 270°C. The results show that the average crystallite size varies between 41 and 61 nm using the (2 0 0) plane with complex (1) (Figure 5(a)) and between 26 and 46 nm using the (2 0 0) plane with complex (2) (Figures 5(a) and 5(b)).

EDX analysis was carried out to verify the composition of the PbS NPs synthesized in the OLA, and the results are

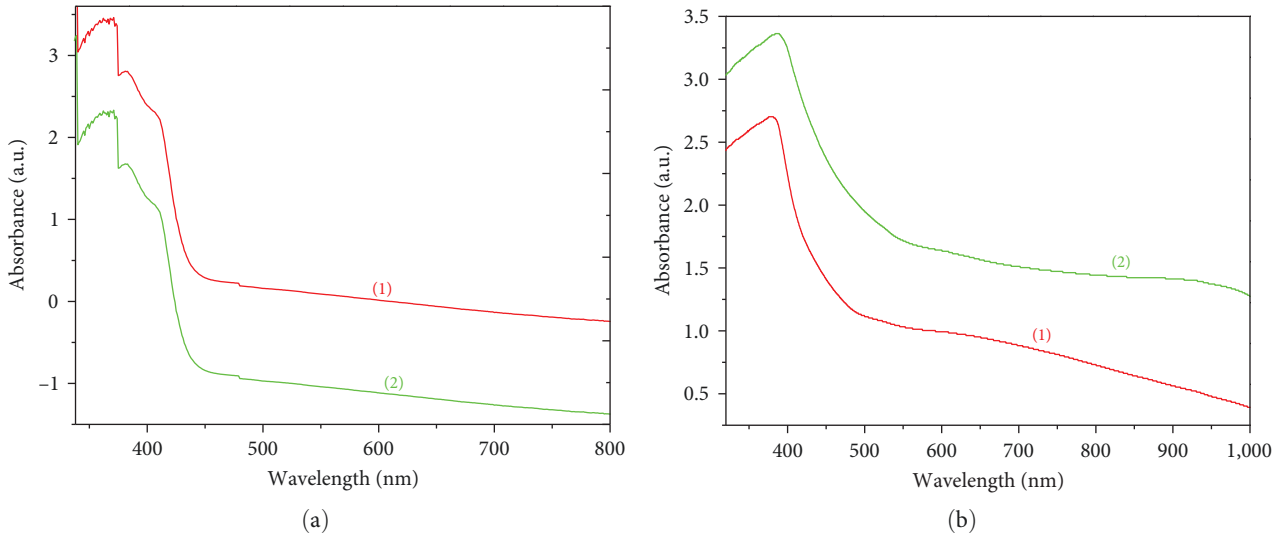

FIGURE 3: UV–visible spectra of (1a) 2-thiophenecarboxaldehyde thiosemicarbazone, (2a) 2-acetylthiophene thiosemicarbazone, and (1b, 2b) its corresponding lead(II) complexes.

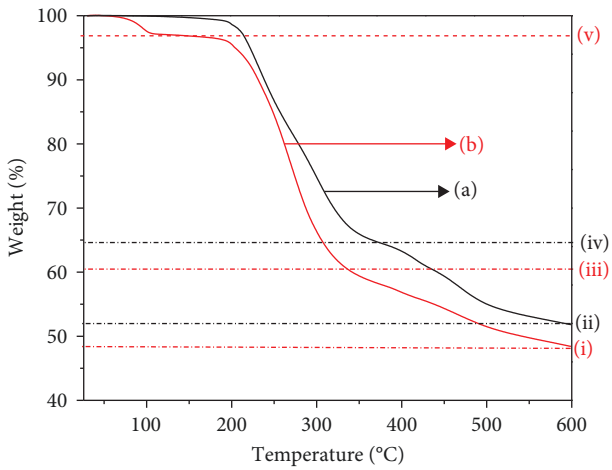

FIGURE 4: TGA analysis for (a) PbL_1 and (b) PbL_2 complexes under nitrogen atmosphere. Roman numerals (i–v) indicate the various decomposition stages.

shown in Figure 6. In addition to certain constituent elements such as the C and O peaks, the EDX spectra reveal the presence of Pb and S. In the EDX spectrum, the observed carbon peaks could be originate from the double-sided carbon ribbon used to analyze the nanoparticles and from oleylamine used as capping agent. PbS NPs were formed, as shown by the presence of Pb and S in the EDX spectrum. The oxygen observed in the EDX spectrum of the PbS NPs may have been absorbed by the ambient air during the preparation of the sample for analysis. A similar pattern was observed in the EDX spectrum (Figure 6(b)), when complex (2) was used as a precursor. These results show that the elemental composition of PbS nanoparticles was not affected by the change in precursor type and the variation in thermolysis temperature.

3.2.2. Morphological Studies of OLA-Capped PbS NPs. TEM and scanning electron microscopy (SEM) analyses were used to investigate the effect of precursor type and reaction temperature on the size and shape of PbS NPs, as illustrated in Figures 7 and 8. The morphologies formed during the synthesis of nanoparticles through the SSP route have been primarily ascribed to the ligands size and functional groups in the precursor [13]. With complex (1), the variation of the reaction temperature did not alter the morphology of PbS NPs. As shown in Figure 7(a)–7(c), cubic-shaped PbS NPs were formed with average sizes of 55, 47, and 65 nm at 190, 230, and 270°C, respectively. This confirmed that the average particle size of the as-prepared PbS NPs is influenced by the thermolysis temperature. Due to the thermodynamic growth regime, no perceptible change in shape was observed by varying the temperature. A variation in particle size was observed as the temperature increased with the smallest size obtained at 230°C. Ostwald ripening process could be responsible for the observed increase in particle size observed between 230 and 270°C [20]. Nanoparticle size is known to be influenced by temperature, with larger particles favored by higher temperatures. The synthesis of cubic-shaped PbS NPs by thermolysis of the lead(II) 2-benzimidazole dithiocarbamate complex has been reported by Thangwane et al. [31] with similar results. The PbS particles obtained in this work are smaller than those reported in a similar study [13], where halogenated and nonhalogenated lead complexes of cinnamaldehyde thiosemicarbazone were used as single source precursors. The formation of PbS NPs in the crystalline cubic phase at different reaction temperatures was confirmed by the diffraction rings in the selected area electron diffraction (SAED) patterns of the synthesized PbS NPs, as shown in Figure 7(g)–7(i) [31]. In addition, the diffraction rings in the SAED pattern of the synthesized PbS NPs, as shown in Figure 7(g)–7(i), also confirm the formation of crystalline cubic phase PbS NPs at different reaction temperatures [32]. With complex (2), where two methyl groups are added in the structure, highly agglomerated and shapeless PbS NPs were formed, regardless of the reaction temperature as shown in

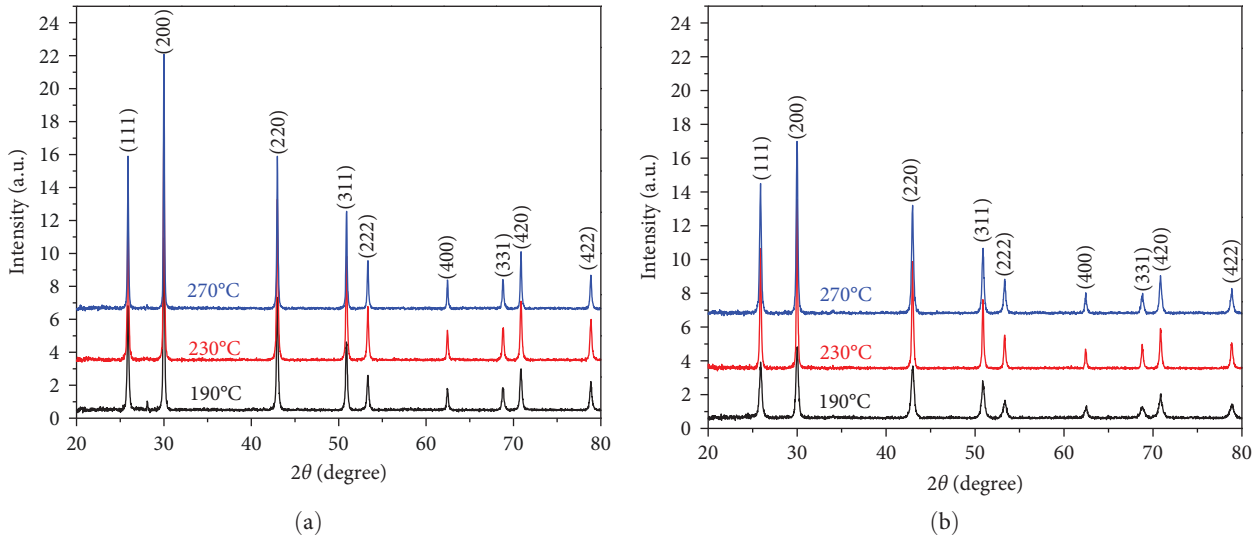

Figure 5: p-XRD spectra of PbS NPs using (a) complex (1) and (b) complex (2) in OLA at different temperatures.

Figure 7(d)–7(f), indicating that the final morphology of the synthesized PbS NPs is influenced by the precursor type. The crystalline nature of the synthesized cubic phase of PbS nanoparticles was further confirmed by the appearance of diffraction rings in the SAED patterns (Figure S1) [32, 33].

Figure 8 shows SEM images of PbS NPs obtained from complexes (1) and (2) as precursors. When complex (1) was thermolyzed at 190 and 230°C, aggregates of PbS NPs were formed (Figures 8(a) and 8(b)). Porous surfaces were observed (Figures 8(a) and 8(b)) with less at 230°C (Figure 8(b)). At higher temperature (270°C), flower like PbS were formed as shown in Figure 8(c). When complex (2) was thermolyzed at 190°C, a mixture of irregular spherical, rod-shaped, and petal-shaped PbS particles were formed, as shown in Figure 8(d). Increasing the reaction temperature to 230 and 270°C gave rise to the formation of agglomerated flower-like seeds with porous surfaces, as shown in Figures 8(e) and 8(f)). The variation in the thermolysis temperature and the change in the type of precursors could be the cause of the variations observed in the surface morphology of PbS NPs. This shows that reaction temperature affects the surface morphology of PbS NPs.

3.2.3. Optical Studies of OLA-Capped PbS Nanoparticles. UV–visible spectroscopy was used to examine the effect of the reaction temperature and the nature of the precursors (complexes) on the optical properties of nanoparticles, as shown in Figure 9. Bandgap energies were estimated using Tauc plots [13, 20]. As shown in Figures 9(b) and 9(d)), the bandgap energies vary from 2.45 to 2.96 eV for complex (1) and from 2.40 to 2.96 eV for complex (2) at different temperatures (190, 230, and 270°C). As PbS NPs are nanometric in size, these energies correspond to a blue shift compared with bulk PbS (0.41 eV). The bandgap energies observed are within the range reported by Masikane et al. [4] and Mubiayi et al. [17]. On the basis of the UV–vis absorption spectra and Tauc plots, as illustrated in Figure 9, these bandgap energies of the as-prepared PbS nanoparticles show that the exciton absorption peaks varied as a function of reaction temperature, with smaller bandgaps being associated with larger particle sizes and vice versa. Similar results on the variation of the energy bandgap of PbS NPs with increasing reaction temperature were observed by Mubiayi et al. [17]. The results indicate that the OLA-coated PbS NPs obtained using complex (1) at 230 and 270°C have similar bandgap energies to those obtained using complex (2). This shows that the optical properties of the synthesized PbS NPs were not affected by the variation in precursor type but influenced by variation in reaction temperature. This could be explained by changes in the size of the lead(II) sulfide nanoparticles as temperature changes. It has been shown that the optical properties of nanoparticles are influenced by their size [17].

3.3. Characterization of HDA-Capped PbS Nanoparticles

3.3.1. Structural Characterization of HDA-Capped PbS Nanoparticles. The carbon chain of the primary amine was reduced from C_{18} to C_{16} by replacing OLA with HDA in order to examine the effect of the capping agent on the structure of PbS NPs. The phase composition and structure of HDA-capped PbS NPs using complexes (1) and (2) were investigated using XRD, as shown in Figure 10. When OLA was by HDA under similar reaction conditions, the cubic phase of PbS (galena) characterized by the diffraction planes (111), (200), (220), (311), (222), (400), and (420) was obtained, which is granted JCPDS file number 01-071-4752. The results indicate that the crystallographic phase of the resulting PbS NPs was not affected by the replacement of OLA by HDA. The results also show that increasing the reaction temperature from 190 to 270°C increases the crystallinity of the PbS nanoparticles. Furthermore, the results show that the crystallographic phase of the resulting PbS NPs was not affected by the replacement of oleylamine by hexadecylamine. The average size calculated from the Debye–Scherrer equation [30] varies between 40.64 and 63.48 nm using complex (1) and 31.00–52.90 nm using complex (2), as shown in Figures 10(a) and 10(b). These

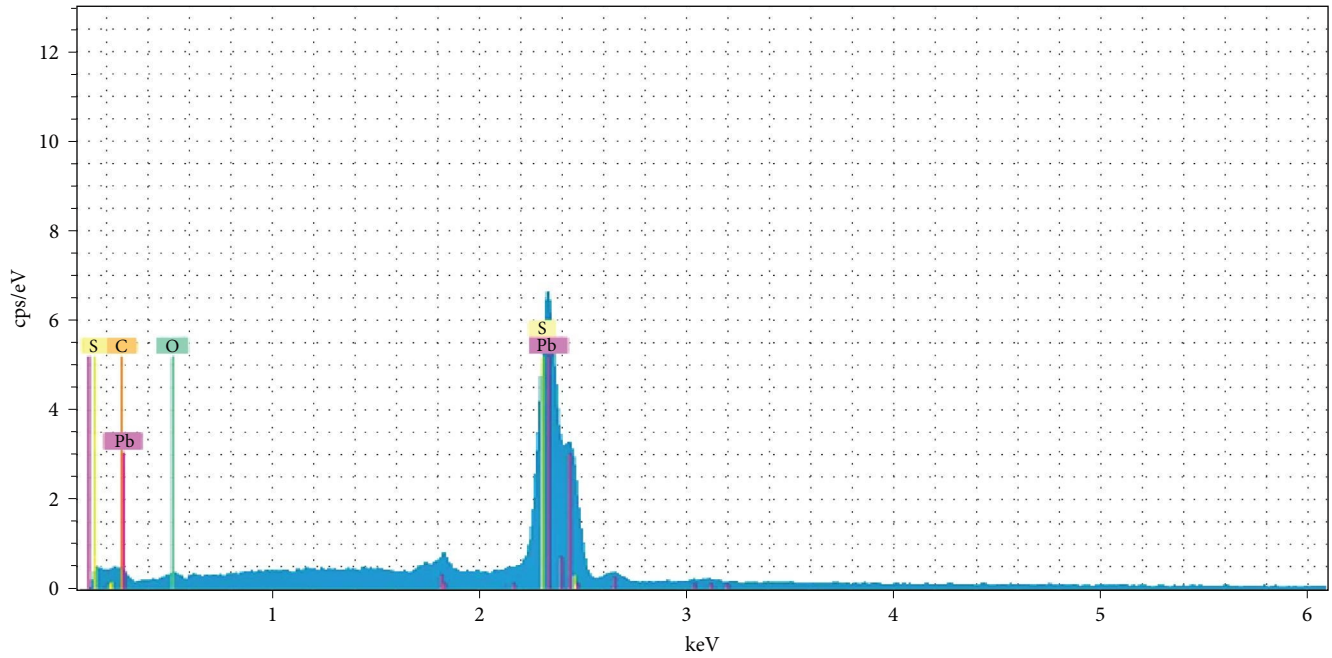

(a)

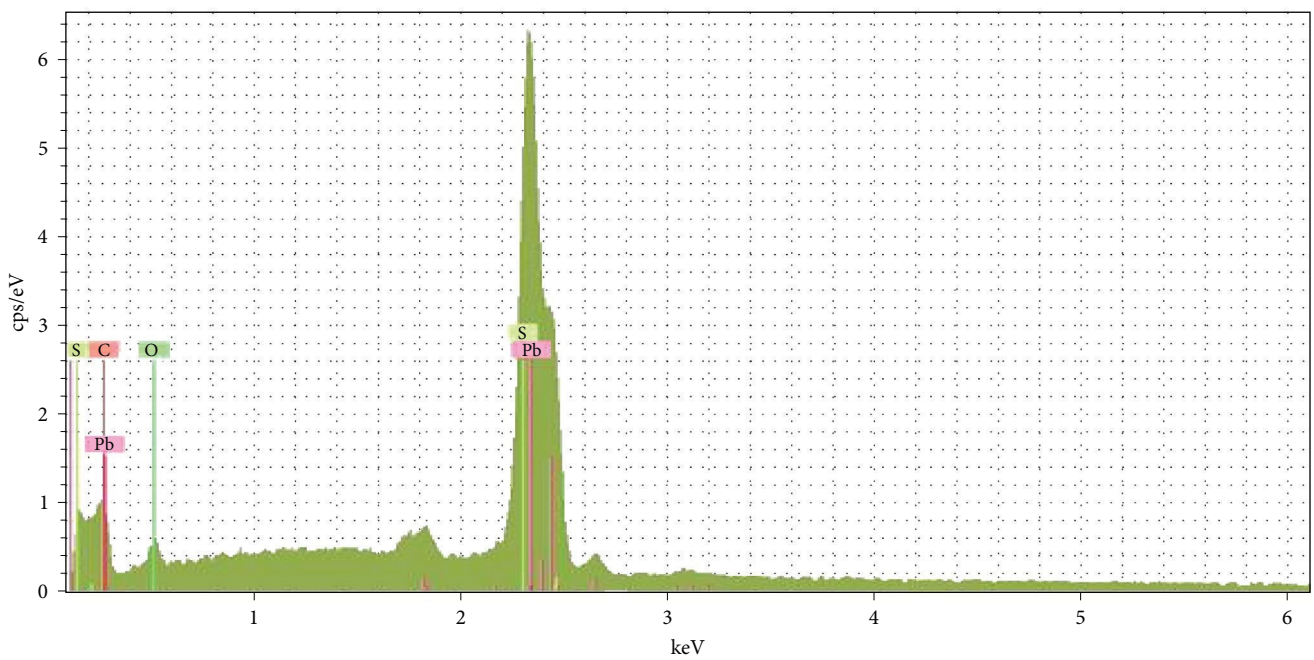

(b)

Figure 6: EDX spectra of PbS nanoparticles from (a) complex (1) and (b) complex (2) at 190°C.

results are comparable with those obtained for OLA-capped PbS NPs.

EDX analysis, as shown in Figure S2, was also used to determine the composition of PbS NPs when hexadecylamine was used as the capping agent. When hexadecylamine was used as capping agent, similar results to those previously reported for OLA-capped PbS NPs were obtained, confirming that thermolysis temperature and a reduction in the length of the carbon chain of the capping agent have no effect on the elemental composition of the lead sulfide nanoparticles contained.

3.3.2. Morphological Studies of HDA-Capped PbS Nanoparticles. It has been reported that hexadecylamine adsorbs dynamically on the growing crystal's surface [34]. The variation of the capping agent from OLA (C_{18} branched primary amine) to HDA

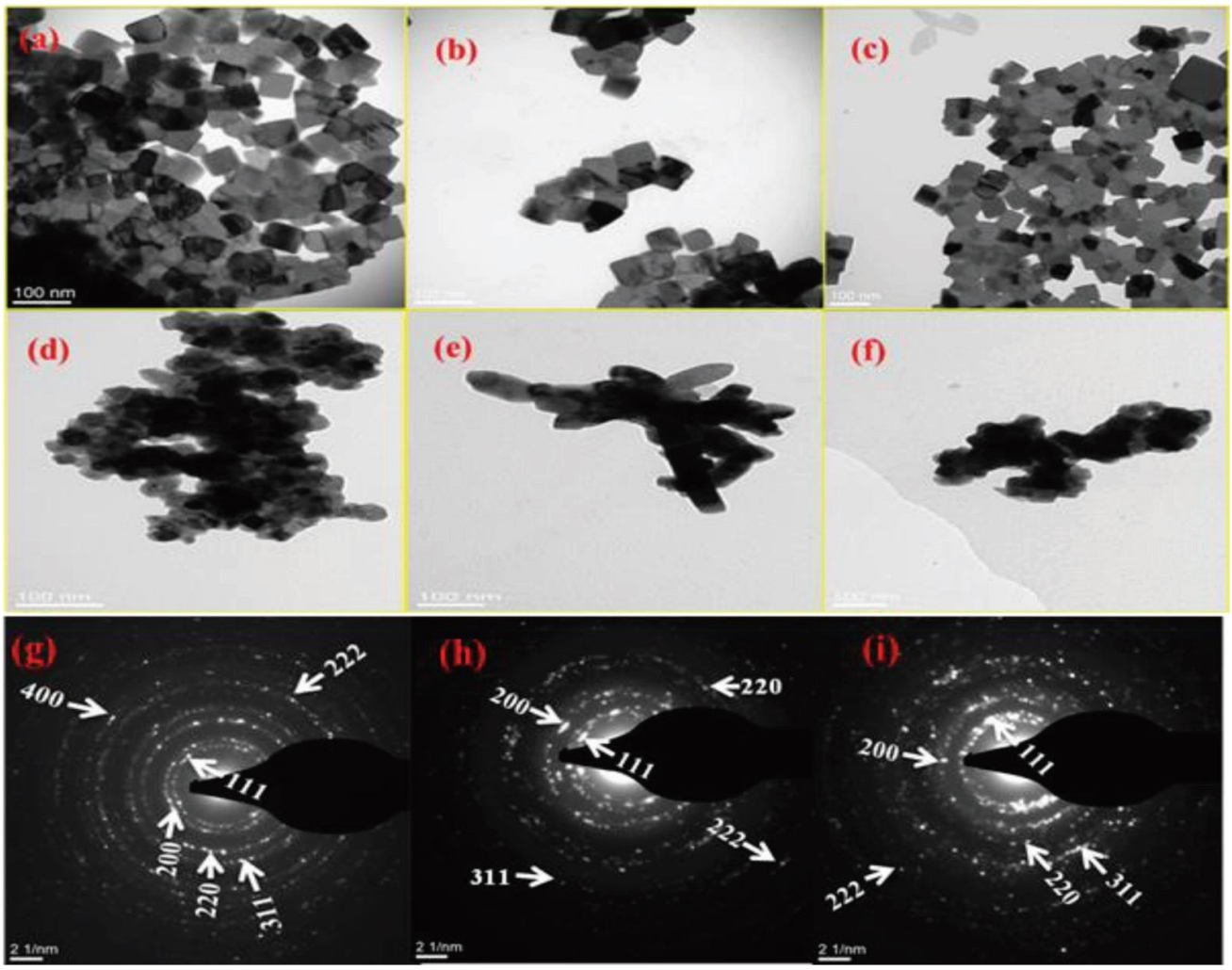

Figure 7: TEM images of PbS NPs obtained from complexes (1) and (2) in OLA at 190°C (a, d), 230°C (b, e), and 270°C (c, f); SAED patterns of nanoparticles prepared at 190, 230, and 270°C from complex (1) (g–i).

(C_{16} linear primary amine) did not influence the final morphology of the synthesized PbS NPs when complex (1) was used. A general variation in the particle size was also observed upon increase of the reaction temperature, suggesting that the variation in thermolysis temperature affects the size of the PbS NPs. As shown in Figure 11(a)–11(c), cubic-shaped PbS NPs with average sizes of around 56, 44, and 68 nm were obtained at 190, 230, and 270°C, respectively. However, when complex (2) was thermolyzed, different morphologies were formed. As shown in Figure 11(d), a mixture of agglomerated cubic and nearly spherical particles with an average size of 26 nm was produced at 190°C. Increasing the reaction temperature to 230°C, cubic-shaped agglomerated PbS NPs with average size of 34 nm were formed, as shown in Figure 11(e). PbS nanorods with an average width of 41 nm were formed when the temperature was raised to 270°C, as shown in Figure 11(f). This result shows that the type of precursor and the increase in temperature influence the final morphology of the PbS NPs. OLA-capped PbS NPs produced at 190 and 230°C were larger than the corresponding HDA-capped PbS NPs and the results are included in Table 3. This observation can be explained by the length of the capping agent alkyl chain, which plays a role in controlling size and shape. It has been reported that crystal morphology can be strongly influenced by the surface energy of nanocrystals by adding a capping agent that adsorbs onto the surfaces of growing particles [4]. At the different reaction temperatures, the PbS NPs are crystalline in nature, as shown by the continuous light spots that produce concentric rings in the electron diffraction patterns of the selective zone (Figure 11(g)–11(i) and Figure S3) [35, 36].

SEM images of PbS NPs from complexes (1) and (2) are shown in Figure S4. Immature dendrite and foil PbS NPs were obtained at 190°C (Figure S4), agglomerated microstructures at 230°C (Figure S4), and nearly spherical agglomerated particles with pores on the surface at 270°C (Figure S4) when complex (1) was used. With complex (2), SEM images showed a less porous surface covered with clusters at 190°C (Figure S4), agglomerated seeds at 230°C (Figure S4) and agglomerated seeds with a porous surface at 270°C (Figure S4). These results show that the surface morphology of the PbS NPs is

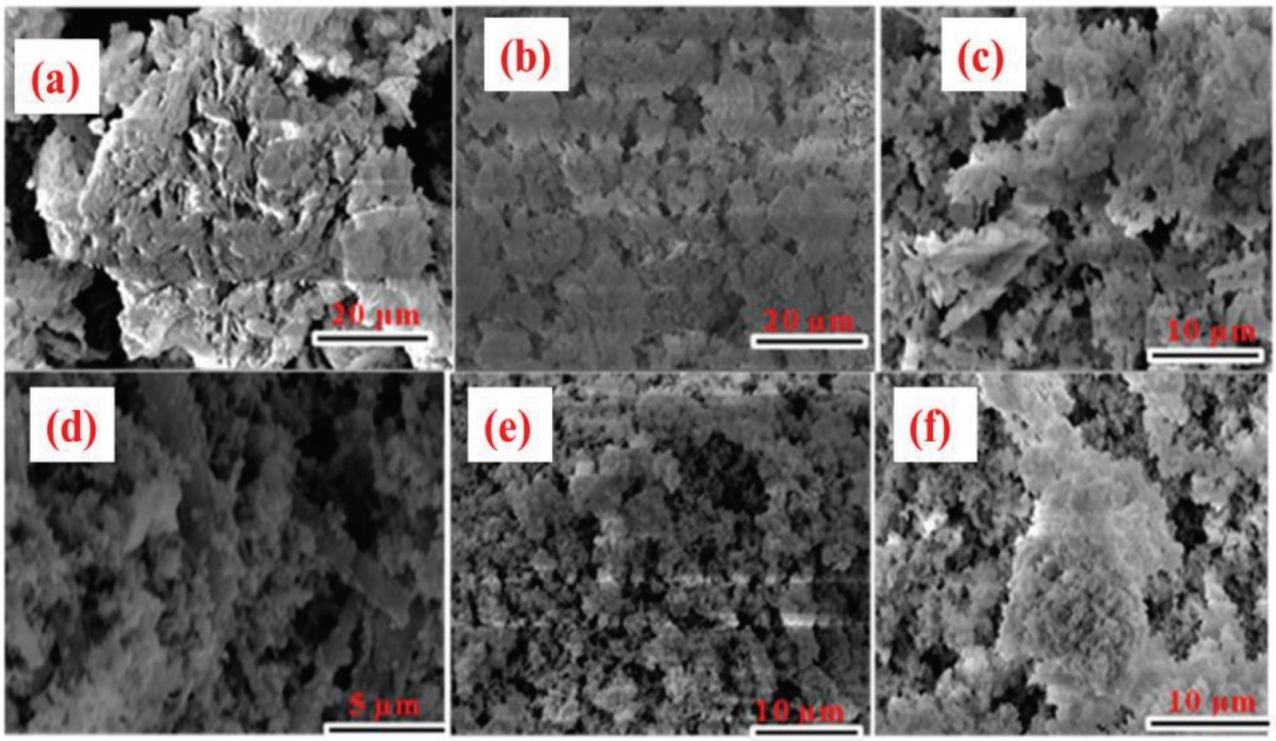

Figure 8: SEM images of PbS NPs obtained from complexes (1) and (2) in OLA at 190°C (a, d), 230°C (b, e), and 270°C (c, f).

affected by an increase in the reaction temperature and a decrease in the length of the carbon chain of the capping agent.

3.3.3. Optical Studies of HDA-Capped PbS NPs. Figure 12 shows the absorption spectra and Tauc plots of HDA-coated PbS NPs obtained at 190, 230, and 270°C. The results show that each PbS nanoparticle obtained exhibited a blue shiftrelative to the bulk PbS material, indicating the formation of nanosized particles [4, 17]. As shown in Figure 12(a)–12(d), the bandgap energies for complex (1) and complex (2) varied between 2.15–2.92 eV and 2.46–3.11 eV at various temperatures. The variation in reaction temperature, the type of precursor, and the carbon chain length of the capping agent affect the optical propertiesof the PbS NPs, as shown by the difference in bandgap energy observed. The bandgaps of OLA-capped PbS NPs are larger than those of HDA-capped PbS NPs with complex (1), while thebandgaps of HDA-capped PbS NPs are larger than those of OLA-capped PbS NPs with complex (2). Reduced nanoparticle size is the reason for the increase in the bandgap. Thangwane et al. [31] obtained similar results to those reported in this work when lead(II) complexes of 2-benzimidazoledithiocarbamate were thermolyzed in HDA and TOPO [36]. Table 3 summarizes the reaction conditions, sizes, shapes, and optical properties of the lead sulfide nanoparticles.

3.4. Photodegradation of Methylene Blue Using HDA-Capped PbS NPs. The photocatalytic activity PbS NPs was examined, based on the photocatalytic degradation of methylene blue dye (MB) under UV irradiation using HDA-capped PbS NPs due to the well-defined shape of HDA-capped PbS NPs compared to those of OLA-capped PbS NPs obtained under similar reaction conditions. Absorption spectra of the MB dye solution containing HDA-capped PbS nanoparticles after exposure to UV irradiation light at 15, 30, 45, and 60 min are shown in Figure S5. As the exposure time increased from 0 to 60 min, absorption intensity peak decreased due to the degradation of MB dye. The PbS NPs elaborated at 190 (PbS-HDA_1) and 230°C (PbS-HDA_2) using complex (1) showed degradation efficiencies of 28.3% and 60%, respectively, after 60 min exposure to UV irradiation. Table 4 shows the maximum degradation efficiency of 48% for PbS NPs obtained at 270°C (PbS-HDA3) after 45 min. The percentage degradation efficiency of PbS nanoparticles obtained at 230°C is higher than those of PbS nanoparticles at 190 and 270°C after 60 min of UV irradiation (Figure 13(a)). When complex (2) was used, degradation efficiencies of 54.4%, 58%, and 50% were obtained for HDA_5-PbS (230°C), HDA_6-PbS (270°C) after 60 min exposure, and PbS-HDA_4 nanoparticles (190°C) after 45 min (Table 4). However, a decrease was observed after 45 min of irradiation with the PbS-HDA_3 and PbS-HDA_4 nanoparticles. This could be explained by the fact that when anionic radicals decrease over time, the rate of degradation also decreases, leading to a drop in the percentage of degradation. When Ali et al. [37] reported on the synthesis of cobalt ferrite nanomaterials for the photocatalytic degradation of Congo red dye, they also noted similar observations. After 60 min of UV irradiation, the PbS nanoparticles obtained at 270°C (PbS-HDA_6) showed a higher degradation rate than the PbS nanoparticles obtained at 230 (PbS-HDA_5) and 190°C (PbS-HDA_4) (Figure 13(b)).

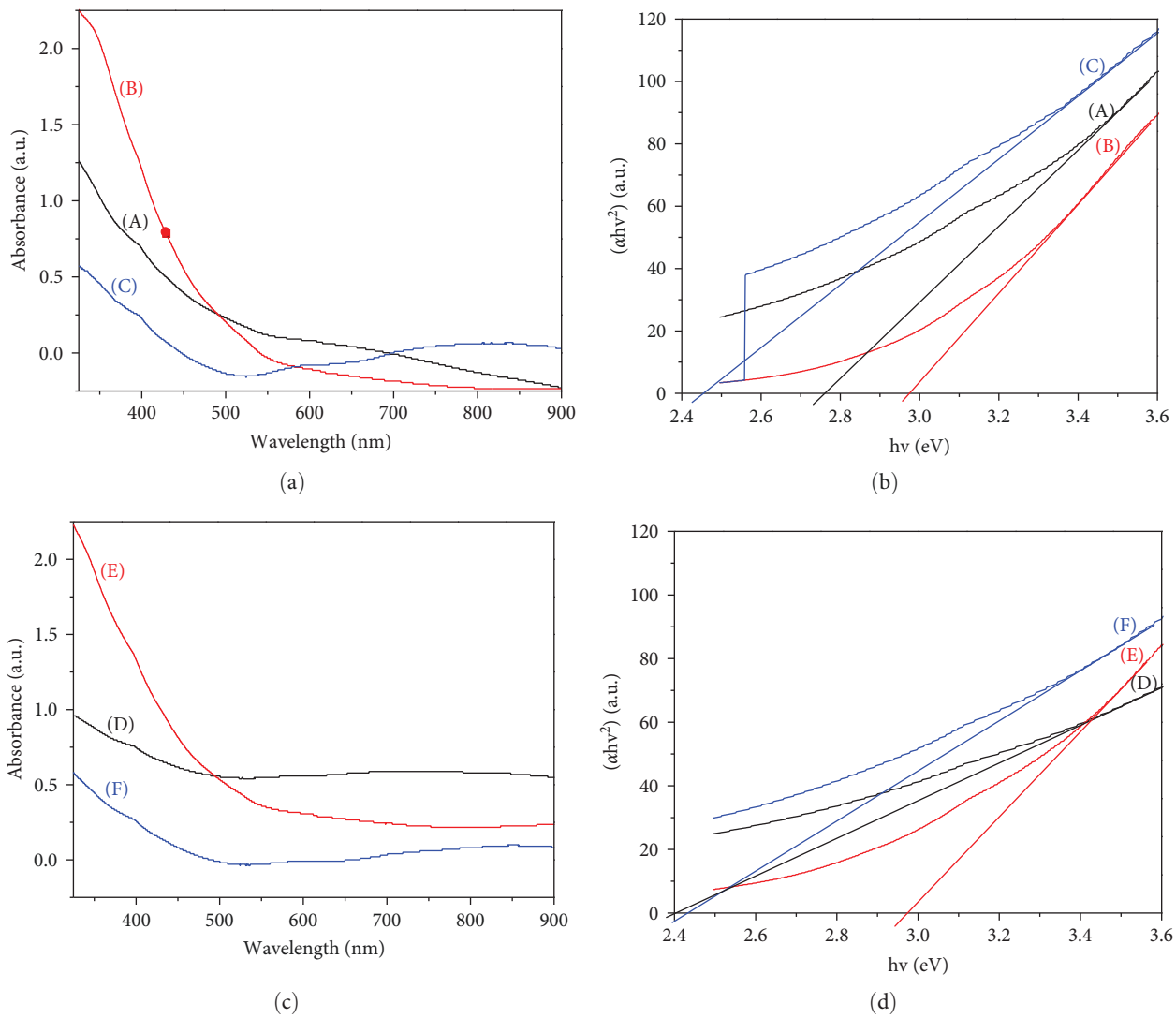

Figure 9: UV–visible-NIR spectra (a, c) and the corresponding Tauc plots (b, d) of PbS nanoparticles prepared in OLA at 190°C (A and D), 230°C (B and E), and 270°C (C and F) using complex (1) (a, b) and complex (2) (c, d).

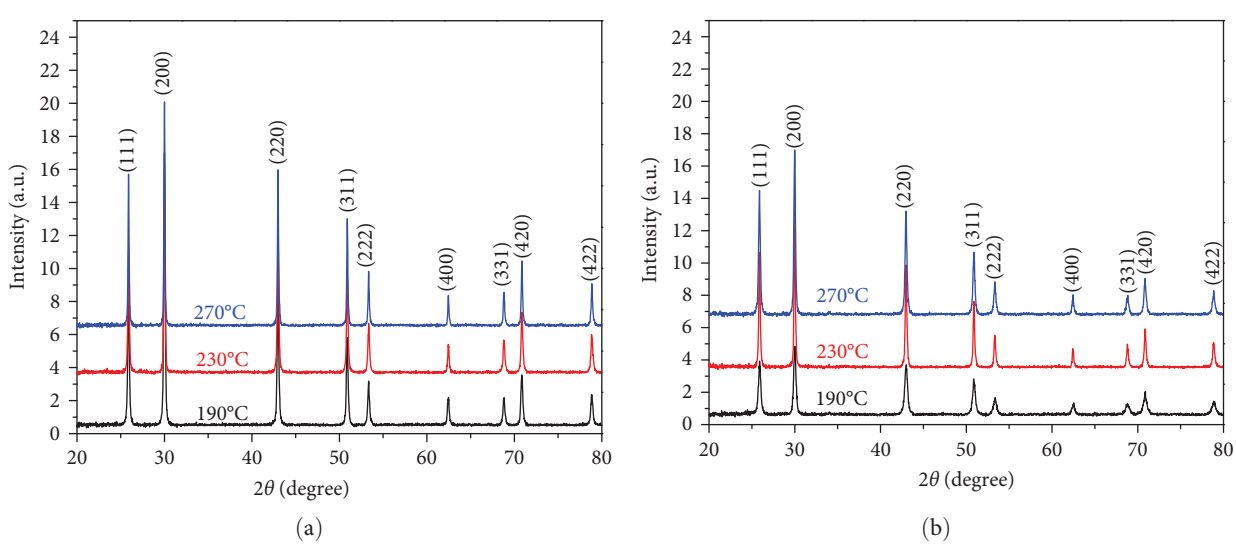

Figure 10: p-XRD spectra of PbS nanoparticles in HDA at different temperature from (a) complex (1) and (b) complex (2).

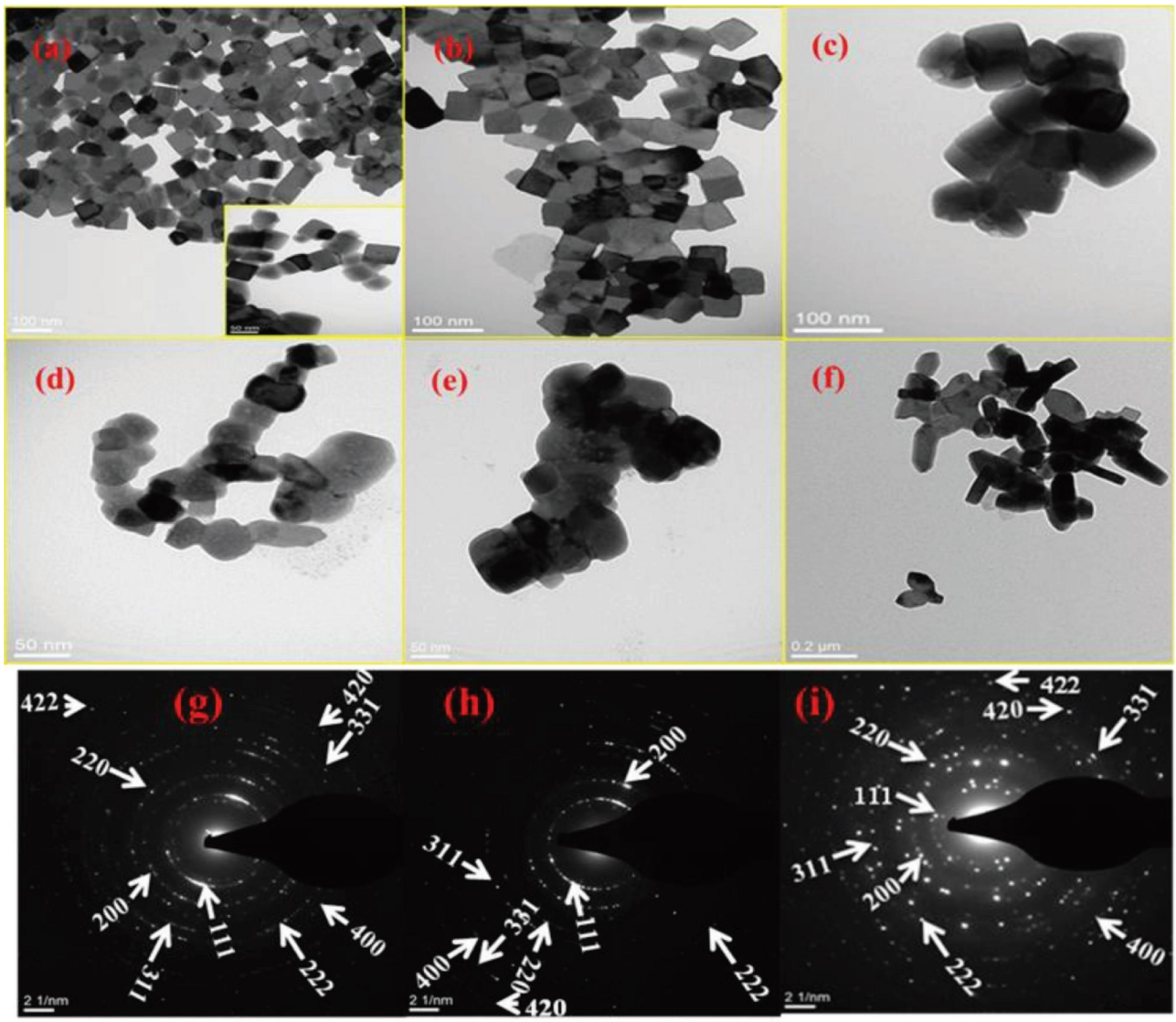

Figure 11: TEM images of PbS NPs obtained from complexes (1) and (2) in HDA at 190°C (a, d), 230°C (b, e), and 270°C (c, f); showing the SAED patterns at 190, 230, and 270°C from complex (1) (g–i).

Table 3: Overview of the size, shape, and optical properties of lead sulfide NPs, as well as the reaction parameters.

Complexes	Dispersion medium	Capping agent	Temperature (°C)	Morphology	Eg (eV)	Average size (nm)
(1)	OLA	OLA	190	Cubic	2.75	55
			230	Cubic	2.96	47
			270	Cubic	2.45	65
		HDA	190	Cubic	2.15	56
			230	Cubic	2.92	44
			270	Cubic	2.42	68
(2)	OLA	OLA	190	—	2.40	—
			230	—	2.96	—
			270	—	2.45	—
		HDA	190	Nearly spherical to cubic	3.11	26
			230	Cubic	2.46	34
			270	Nanorods	2.97	41

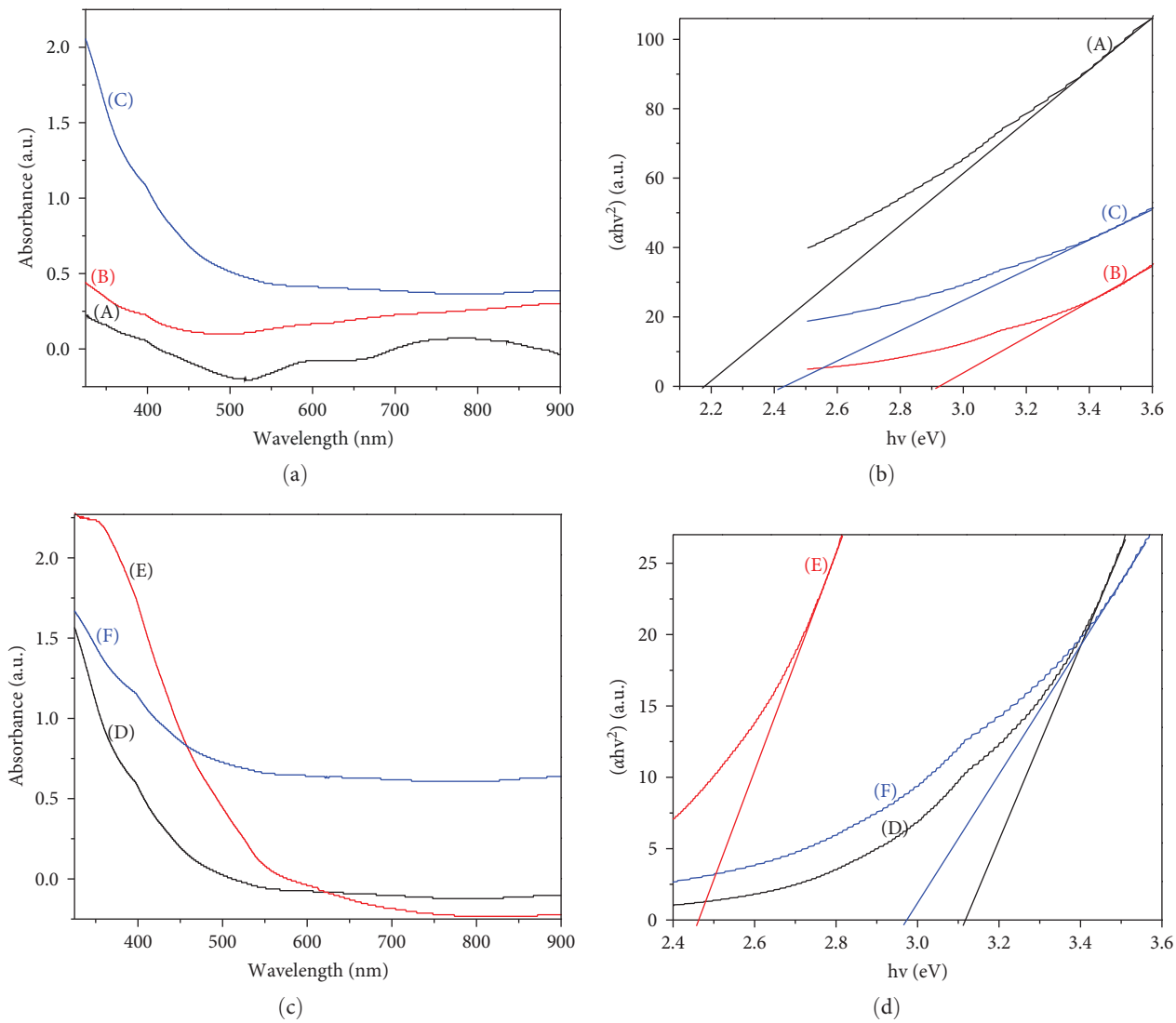

Figure 12: UV–visible-NIR spectra (a, c) and Tauc plots (b, d) of PbS NPs obtained in HDA using complex (1) (a, b) and complex (2) (c, d) at 190°C (A and D), 230°C (B and E), and 270°C (C and F).

Table 4: Efficiency of HDA-capped PbS NPs degradation using complexes (1) and (2).

		Complex (1) as single source precursor			
	Times (min)	15	30	45	60
PbS-HDA$_1$	η (%)	14.0	23.5	24.1	28.3
PbS-HDA$_2$	η (%)	46.4	49.0	55.0	60.0
PbS-HDA$_3$	η (%)	40.0	47.0	48.0	45.2
		Complex (2) as single source precursor			
PbS-HDA$_4$	η (%)	42.0	45.2	50.0	42.0
PbS-HDA$_5$	η (%)	40.4	42.2	53.0	54.4
PbS-HDA$_6$	η (%)	41.0	45.2	50.0	58.0

The reaction temperature and precursor type could have influenced the photocatalytic properties of PbS NPs [36]. One possible explanation for the high degradation efficiency of PbS-HDA$_6$ (58%) and PbS-HDA$_2$ (60%) nanoparticles is that their surfaces are porous, as it has been reported that a porous surface favors an increase in the photocatalytic activity of NPs due to the active sites available [36]. The degradation efficiencies values obtained here are relatively close to those reported by Mishra and Saha [38]. The number of electron–hole pairs generated that can react on the surface of PbS NPs determines the efficiency of MB degradation. Thus, under irradiation conditions, the material should facilitate electron–hole

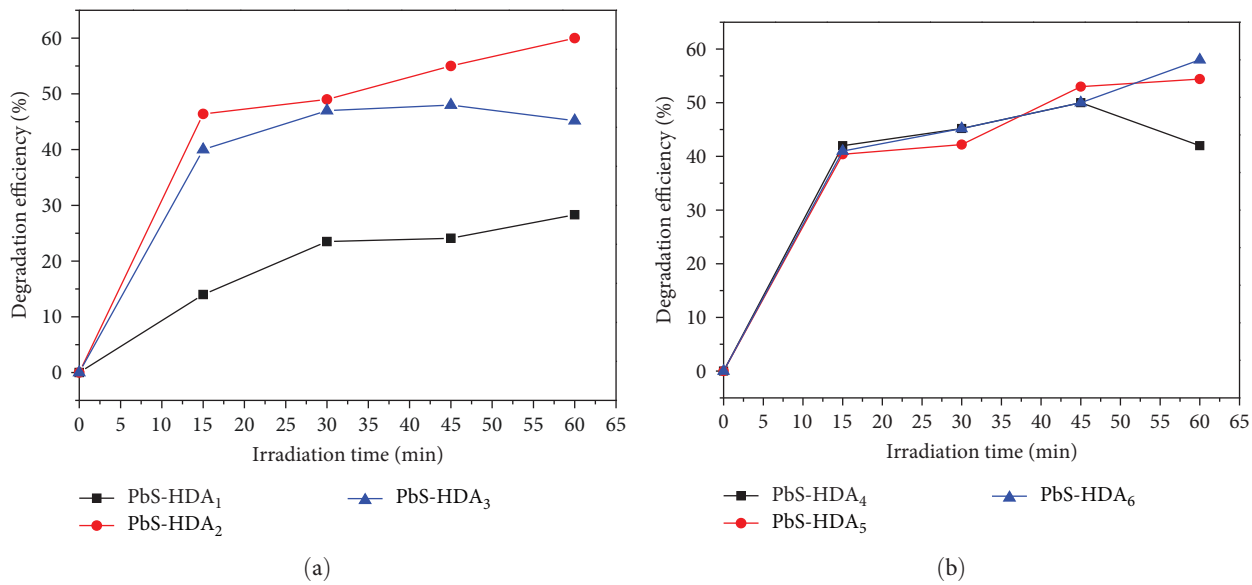

Figure 13: MB degradation efficiency curves using (a) complex (1) and (b) complex (2) at ($PbS\text{-}HDA_1$, $PbS\text{-}HDA_4$) 190, ($PbS\text{-}HDA_2$, $PbS\text{-}HDA_5$) 230, and ($PbS\text{-}HDA_3$, $PbS\text{-}HDA_6$) 270°C at various irradiation times.

Table 5: Methylene blue dye degradation using metal sulfide photocatalyst.

Metal sulfide catalysts	Ligth source	Irradiation time	Degradation rate (%)	Reference
PbS	70 W, mercury lamp	3 hr	72.6, 75.9, and 47.4	[32]
ZnS	8 W, ultraviolet lamp	6 hr	27	[39]
PbS	3 kW/m^2 direct light	1 hr	50, 56, and 60	[38]
$Cu_{1.8}S$	70 W, mercury	3 hr	42.52	[40]
FeS_2	400 W, halogen	3 hr 30 min	13.2	[41]
Ag_2S	70 W, mercury	3 hr	48.39	[40]
PbS	15 W, UV–vis radiation	3 hr	25	[42]
Ag–PbS	15 W, UV–vis radiation	3 hr	68	[42]
CuS	125 W, mercury	1 hr	33	[43]
Cu_9S_5	60 W/m^2, UV light	1 hr 30 min	80	[22]
CdS	High-pressure sodium lamp	3 hr	54–76 11–47 40–61	[44] [44]
PbS	60 W/m^2, UV light	1 hr	60	This work

separation and inhibit charge carrier recombination, allowing the production of additional oxidizing species, such as oxygen and hydroxyl radicals, which then function as active centers to react with the organic dye to oxidize it. Table 5 summarizes the results of degradation efficiencies of MB, reported using other metal sulfide NPs. This table shows that in most of the cases, the light intensity and time required for MB degradation is greater than in the present results. Based on the high degradation efficiency of HDA-coated PbS NPs, lead sulfide nanoparticles can be used as effective photocatalysts for removing organic pollutants from water effluents.

4. Conclusion

The thermolysis of two lead(II) thiosemicarbazone complexes in two primary amine capping molecules at 190, 230, and 270°C yielded lead sulfide NPs. PbS nanoparticles in their prepared form have a cubic crystalline phase of rock salt and a cubic, rod-shaped, almost spherical morphology. Compared with the bandgap energy of bulk PbS, the optical properties of PbS nanoparticles show a blue shift. While the optical properties depend on the solvent and the type of precursor, the shape and size of the PbS NPs depend on the temperature and the solvent. After 60 min of irradiation with UV light, the results showed that the HDA-coated PbS nanoparticles obtained at 230°C using complex (1) were effective photocatalysts for the degradation of methylene blue dye at a rate of 60%.

Data Availability

The data used to support the results of this study are presented in the paper. The corresponding author can provide any additional information upon request.

Conflicts of Interest

The authors declare that they have no conflicts of interest.

Acknowledgments

The authors acknowledge the mobility bursary provided to APY by the Institute Jean Lamour of the University of Lorraine (France). They also thank the University of Zululand (Department of Chemistry) for some of the analysis. This work received financial assistance to acquire reagents, under the allocation, Fond de modernisation et d'appui a la recherche, to University Teachers of Cameroon.

Supplementary Materials

Figure S1: SAED patterns of nanoparticles prepared in OLA at 190, 230, and 270°C from complex (2). Figure S2: EDX spectra of PbS nanoparticles prepared in HDA at 190°C using complexes (1) and (2). Figure S3: SAED patterns of Nps prepared in HDA at 190, 230, and 270°C from complex (2). Figure S4: SEM images of PbS Nps prepared in HDA at 190°C (a, d), 230°C (b, e), 270°C (c, f) using complexes (1) and (2). Figure S5: UV–vis absorption spectra of (HDA)-capped PbS nanoparticles used in the photodegradation of methylene blue. (*Supplementary Materials*)

References

[1] S. Shen and Q. Wang, "Rational tuning the optical properties of metal sulfide nanocrystals and their applications," *Chemistry of Materials*, vol. 25, no. 8, pp. 1166–1178, 2013.

[2] M. Salavati-Niasari, A. Sobhani, and F. Davar, "Synthesis of star-shaped PbS nanocrystals using single-source precursor," *Journal of Alloys and Compounds*, vol. 507, no. 1, pp. 77–83, 2010.

[3] L. D. Nyamen, V. S. R. Rajasekhar Pullabhotla, A. A. Nejo, P. T. Ndifon, J. H. Warner, and N. Revaprasadu, "Synthesis of anisotropic PbS nanoparticles using heterocyclic dithiocarbamate complexes," *Dalton Transactions*, vol. 41, no. 27, pp. 8297–8302, 2012.

[4] S. C. Masikane, S. Mlowe, C. Gervas, N. Revaprasadu, A. S. Pawar, and S. S. Garje, "Lead(II) halide cinnamaldehyde thiosemicarbazone complexes as single source precursors for oleylamine-capped lead sulfide nanoparticles," *Journal of Materials Science: Materials in Electronics*, vol. 29, no. 2, pp. 1479–1488, 2018.

[5] D. C. Onwudiwe and V. M. Nkwe, "Morphological variations in Bi_2S_3 nanoparticles synthesized by using a single source precursor," *Heliyon*, vol. 6, no. 7, Article ID e04505, 2020.

[6] D. C. Onwudiwe, "Microwave-assisted synthesis of PbS nanostructures," *Heliyon*, vol. 5, no. 3, Article ID e01413, 2019.

[7] P. Uddandarao and R. Mohan, "ZnS semiconductor quantum dots production by an endophytic fungus *Aspergillus flavus*," *Materials Science and Engineering: B*, vol. 207, pp. 26–32, 2016.

[8] K. Veerathangam, M. S. Pandian, and P. Ramasamy, "Synthesis and characterization of cadmium sulfide (CdS) quantum dots (QDs) for quantum dot sensitized solar cell applications," *International Journal of ChemTech Research*, vol. 6, no. 13, pp. 5396–5399, 2014.

[9] P. A. Ajibade and A. E. Oluwalana, "Structural, optical, photocatalytic and electrochemical studies of PbS nanoparticles," *Journal of Nano Research*, vol. 61, pp. 18–31, 2020.

[10] M. Atwa, A. Al-Kattan, and A. Elwan, "Towards nano architecture: nanomaterial in architecture—a review of functions and applications," *International Journal of Recent Scientific Research*, vol. 6, no. 4, pp. 3551–3564, Article ID 012121, 2015.

[11] A. Ekinci, Ö. Şahin, and S. Horoz, "Chemical bath deposition of Co-doped PbS thin films for solar cell application," *Journal of Materials Science: Materials in Electronics*, vol. 31, no. 2, pp. 1210–1215, 2019.

[12] Z. Mamiyev and N. O. Balayeva, "PbS nanostructures: a review of recent advances," *Materials Today Sustainability*, vol. 21, Article ID 100305, 2023.

[13] I. Jen-La Plante, T. W. Zeid, P. Yang, and T. Mokari, "Synthesis of metal sulfide nanomaterials via thermal decomposition of single-source precursors," *Journal of Materials Chemistry*, vol. 20, no. 32, pp. 6612–6617, 2010.

[14] C. Song, M. Sun, Y. Yin et al., "Synthesis of star-shaped lead sulfide (PbS) nanomaterials and theirs gas-sensing properties," *Materials Research*, vol. 19, no. 6, pp. 1351–1355, 2016.

[15] P. D. McNaughter, S. A. Saah, M. Akhtar et al., "The effect of alkyl chain length on the structure of lead(II) xanthates and their decomposition to PbS in melt reactions," *Dalton Transactions*, vol. 45, no. 41, pp. 16345–16353, 2016.

[16] J. O. Adeyemi and D. C. Onwudiwe, "PbS nanoparticles prepared using 1, 10-phenanthroline adduct of lead(II) bis(N-alkyl-N-phenyl dithiocarbamate) as single source precursors," *Molecules*, vol. 25, no. 9, Article ID 2097, 2020.

[17] K. P. Mubiayi, N. Revaprasadu, S. S. Garje, and M. J. Moloto, "Designing the morphology of PbS nanoparticles through a single source precursor method," *Journal of Saudi Chemical Society*, vol. 21, no. 5, pp. 593–598, 2017.

[18] J. C. Sarker and G. Hogarth, "Dithiocarbamate complexes as single source precursors to nanoscale binary, ternary and quaternary metal sulfides," *Chemical Reviews*, vol. 121, no. 10, pp. 6057–6123, 2021.

[19] A. M. Paca and P. A. Ajibade, "Optical and structural studies of iron sulphide nanoparticles and iron sulphide hydroxyethyl cellulose nanocomposites from bis-(dithiocarbamato) iron(II) single-source precursors," *Nanomaterials*, vol. 8, no. 4, Article ID 187, 2018.

[20] A. E. Oluwalana and P. A. Ajibade, "Synthesis and crystal structures of Pb(II) dithiocarbamates complexes: precursors for PbS nanophotocatalyst," *Journal of Sulfur Chemistry*, vol. 41, no. 2, pp. 182–199, 2019.

[21] A. S. Pawar, S. C. Masikane, S. Mlowe, S. S. Garje, and N. Revaprasadu, "Preparation of CdS nanoparticles from thiosemicarbazone complexes: morphological influence of chlorido and iodido ligands," *European Journal of Inorganic Chemistry*, vol. 2016, no. 3, pp. 366–372, 2015.

[22] A. P. Yepseu, T. Girardet, L. D. Nyamen et al., "Copper (II) heterocyclic thiosemicarbazone complexes as single-source precursors for the preparation of Cu_9S_5 nanoparticles: application in photocatalytic degradation of methylene blue," *Catalysts*, vol. 12, no. 1, Article ID 61, 2022.

[23] E. C. Lisic, V. G. Rand, L. Ngo et al., "Cu(II) propionyl-thiazole thiosemicarbazone complexes: crystal structure, inhibition of human topoisomerase IIα, and activity against breast cancer cells," *Open Journal of Medicinal Chemistry*, vol. 8, no. 2, pp. 30–46, 2018.

[24] E. J. Siddiqui, I. Azad, A. R. Khan, and T. Khan, "Thiosemicarbazone complexes as versatile medicinal chemistry agents: a

review," *Journal of Drug Delivery & Therapeutics*, vol. 9, no. 3, pp. 689–703, 2019.

[25] P. A. Ajibade, A. E. Oluwalana, B. M. Sikakane, and M. Singh, "Structural, photocatalytic and anticancer studies of hexadecylamine capped ZnS nanoparticles," *Chemical Physics Letters*, vol. 755, Article ID 137813, 2020.

[26] A. A. Ali, H. Nimir, C. Aktas et al., "Organoplatinum (II) complexes with 2-acetylthiophene thiosemicarbazone: synthesis, characterization, crystal structures, and in vitro antitumor activity," *Organometallics*, vol. 31, no. 6, pp. 2256–2262, 2012.

[27] M. N. Uddin, D. A. Chowdhury, M. M. Rony, and M. E. Halim, "Metal complexes of schiff bases derived from 2-thiophenecarboxaldehyde and mono/diamine as the antibacterial agents," *Modern Chemistry*, vol. 2, no. 2, pp. 6–14, 2014.

[28] El-S. Fathy, El-A. Bishoy, S. Tarek, S. Ghada, A. M. K. Shaden, and R. E. S. Hesham, "Synthesis, characterization, and in vivo anti-cancer activity of new metal complexes derived from isatin-n(4)antipyrinethiosemicarbazone ligand against ehrlich ascites carcinoma cells," *Molecules*, vol. 24, no. 18, pp. 2–25, 2019.

[29] Z. Tshemese, M. D. Khan, S. Mlowe, and N. Revaprasadu, "Synthesis and characterization of PbS nanoparticles in an ionic liquid using single and dual source precursors," *Materials Science and Engineering: B*, vol. 227, pp. 116–121, 2018.

[30] A. E. Oluwalana and P. A. Ajibade, "Structural, optical and photocatalytic studies of hexadecylamine-capped lead sulfide nanoparticles," *International Journal of Industrial Chemistry*, vol. 11, no. 4, pp. 249–260, 2020.

[31] C. S. Thangwane, T. Xaba, and M. J. Moloto, "Influence of temperature and capping molecules on synthesis of cubic structured lead sulfide nanoparticles from substituted benzimidazole dithiocarbamate complex," *Asian Journal of Chemistry*, vol. 29, no. 12, pp. 2711–2716, 2017.

[32] A. E. Oluwalana and P. A. Ajibade, "Structural, optical and photocatalytic studies of oleylamine capped PbS nanoparticles," *Optical and Quantum Electronics*, vol. 53, no. 1, pp. 1–13, 2021.

[33] L. S. Chongad, A. Sharma, M. Banerjee, and A. Jain, "Synthesis of lead sulfide nanoparticles by chemical precipitation method," *Journal of Physics: Conference Series*, vol. 755, Article ID 012032, 2016.

[34] A. E. Oluwalana and P. A. Ajibade, "Effect of temperature and capping agents on structural and optical properties of tin sulphide nanocrystals," *Journal of Nanotechnology*, vol. 2019, Article ID 8235816, 11 pages, 2019.

[35] D. Kuang, A. Xu, Y. Fang, H. Liu, C. Frommen, and D. Fenske, "Surfactant-assisted growth of novel PbS dendritic nanostructures via facile hydrothermal process," *Journal of Advanced Materials*, vol. 15, no. 20, pp. 1747–1750, 2003.

[36] M. Pal, N. R. Mathews, E. Sanchez-Mora, U. Pal, F. P. Delgado, and X. Mathew, "Synthesis of CuS nanoparticles by a wet chemical route and their photocatalytic activity," *Journal of Nanoparticle Research*, vol. 17, no. 301, pp. 1–13, 2015.

[37] N. Ali, A. Said, F. Ali et al., "Photocatalytic degradation of Congo red dye from aqueous environment using cobalt ferrite nanostructures: development, characterization, and photocatalytic performance," *Water, Air, & Soil Pollution*, vol. 231, no. 2, pp. 2–16, 2020.

[38] A. K. Mishra and S. Saha, "Comparison of photocatalytic activity of methylene blue in the presence of different shape lead sulfide nanoparticles," *International Journal of Metallurgical & Materials Science and Engineering*, vol. 10, no. 1, pp. 13–20, 2020.

[39] M. Mehrabian and Z. Esteki, "Degradation of methylene blue by photocatalysis of copper assisted ZnS nanoparticle thin films," *Optik*, vol. 130, pp. 1168–1172, 2017.

[40] P. A. Ajibade, B. M. Sikakane, N. L. Botha, A. E. Oluwalana, and B. Omondi, "Synthesis and crystal structures of bis (dibenzyl dithiocarbamato) Cu(II) and Ag(I) complexes: precursors for $Cu_{1.8}S$ and Ag_2S nano-photocatalysts," *Journal of Molecular Structure*, vol. 1221, Article ID 128791, 2020.

[41] F. Long, J. He, M. Zhang et al., "Microwave-hydrothermal synthesis of Co-doped FeS_2 as a visible-light photocatalyst," *Journal of Materials Science*, vol. 50, no. 4, pp. 1848–1854, 2015.

[42] N. F. Andrade Neto, Y. G. Oliveira, C. A. Paskocimas, M. R. D. Bomio, and F. V. Motta, "Increase of antimicrobial and photocatalytic properties of silver-doped PbS obtained by sonochemical method," *Journal of Materials Science: Materials in Electronics*, vol. 29, no. 22, pp. 19052–19062, 2018.

[43] Y. Y. Lu, Y. Y. Zhang, J. Zhang et al., "In situ loading of CuS nanoflowers on rutile TiO2 surface and their improved photocatalytic performance," *Applied Surface Science*, vol. 370, pp. 312–319, 2016.

[44] P. A. Ajibade, A. E. Oluwalana, and L. L. R. Mphahlele, "Efect of temperature on the morphological, optical, and photocatalytic properties of CdS quantum dots," *Optical and Quantum Electronics*, vol. 53, pp. 2–12, 2021.